P8B.2 A STATISTICAL EVALUATION OF THE SMPRF RANGE-VELOCITY AMBIGUITY MITIGATION TECHNIQUE

J.C. Hubbert*, E. Ruzanski[1] and V. Chandrasekar[1]
*National Center for Atmospheric Research, Boulder, Colorado
[1] Colorado State University, Fort Collins, Colorado

1. INTRODUCTION

Range-velocity ambiguity is a long standing problem of pulsed radar systems and is major issue in weather radar data quality. For uniformly spaced transmit pulses, the maximum unambiguous range is given by, $r_a = cT/2$ where c is the speed of light and T is the PRT (Pulse Repetition Time), while the unambiguous velocity (or Nyquist velocity) is given by $v_a = \lambda/4T$ where λ is the radar wavelength. These two equations are combined to express the so called range-velocity dilemma as,

$$r_a v_a = \frac{\lambda c}{8}. \quad (1)$$

Thus for a fixed wavelength, the product $r_a v_a$ must be constant. Increasing $r_a\,(v_a)$ necessarily decreases $v_a\,(r_a)$. Also, as seen from the definitions of r_a and v_a, as T increases, r_a increases while v_a decreases and vice versa. As a reference point, consider a typical PRT of 1 ms at S-band which yields $v_a = 25\,\mathrm{ms}^{-1}$ and $r_a = 150\,\mathrm{km}$. Clearly weather phenomena routinely exceed both of these values. At low elevation angle scans, radar echoes can be present out to about 460 km if 18 km agl (above ground level) is used to define cloud top, taking the earth's curvature into consideration. The velocity of weather echoes can exceed $40\,\mathrm{ms}^{-1}$ (about 89 MPH) but $40\,\mathrm{ms}^{-1}$ is usually considered a sufficient maximum unambiguous velocity (e.g., $v_a = 40\,\mathrm{ms}^{-1}$ is the FAA requirement for TDWR). An unambiguous range of 460 km requires $T = 3.07$ ms whereas an unambiguous velocity of $40\,\mathrm{ms}^{-1}$ requires $T = 0.625$ ms. The use of higher transmit frequencies further exacerbates this discrepancy by decreasing v_a.

Several techniques exist to ameliorate the effects of range-velocity ambiguity in weather radar and they can be generally divided into four types: 1) phase coding of the transmitted pulses, 2) dual or staggered PRT, 3) multi-PRF (pulse repetition frequency) and 4) polarization diversity pulse pair.

Recently a new multi staggered PRT technique has been proposed for range-velocity ambiguity resolution called SMPRF (Simultaneous Multiple Pulse Repetition Frequency) (Pirtilla et al. 2005). Several different PRTs are chosen and are concatenated to form a block of PRTs, which are repeated in time. Thus, the time length of the block of PRTs is (neglecting the transmit pulse width) $T = T_1 + T_2 + ... + T_i$ where i is the number of unique PRTs in the block and T is typically chosen to be equal to or exceed the desired unambiguous range. A block of pulses separated by the selected PRTs is repeatedly transmitted according to the desired dwell time. Time series with spacing of T are constructed for each sample time and typically consist of echoes from several resolution volumes. The SMPRF algorithm then uses a matrix inversion technique to solve the set of simultaneous equations in order to obtain the power estimates for each resolution volume. The set of constructed time series can also be used to generate unequally spaced samples of the auto correlation function for each resolution volume from which the velocity is estimated. The theory of the SMPRF technique is presented in (Pirtilla et al. 2005) where the technique is illustrated with experimental C-band radar data.

This paper presents a detailed statistical evaluation of the SMPRF recovered mean power and velocity estimates using simulated data and examines issues limiting their recovery. First, the theory of SMPRF is reviewed and the mean power and mean velocity recovery techniques are described. Next, the simulation procedure for constructing the time series is developed. The simulated time series are then used to evaluated the mean error and standard deviation of the SMPRF recovered mean power and velocity estimates for a particular SMPRF scheme. The effect of finite length time series on the SMPRF algorithm recovery performance is discussed.

2. THE SMPRF ALGORITHM

The SMPRF algorithm entails transmission of multiple pulses at different PRTs to extend the maximum unambiguous measurement range and velocity. Transmission of this set, or block, of PRTs is repeated and translates to the dwell time of the radar measurements. Equally-spaced time series are are constructed from the radar echoes from which moment estimates are recovered.

To illustrate the operation of the SMPRF algorithm, consider the example given in (Pirtilla et al. 2005). This

*NCAR/EOL, Boulder, Colorado 80307, email: hubbert@ucar.edu

code is comprised of four PRTs: 750μs, 1200μs, 1500μs, and 1050μs. To simplify notation these PRTs are normalized by the greatest common divisor of the PRTs, namely $\Delta_t = 150\mu$s. The normalized PRTs are 5, 8, 10 and 7, respectively, and these normalized PRTs are referred to as the SMPRF code which is annotated as "SMPRF$_{(150);5,8,10,7}$".

A diagram of a block of pulses of the SMPRF$_{(150);5,8,10,7}$ code is shown in Fig. 1. The axis is labeled in normalized time units and the first time series sample occurs at $t = 1$. Pulses are transmitted at times $t = 0, -7, -17, -25$ and -30. The pulse at $t = 0$ marks the beginning of the repetition of the PRT block shown at times $t = -30$ through $t = -1$. Thus, the block of PRTs then continues with pulses occurring at times $t = 0 + 30i$, $5 + 30i$, $13 + 30i$ and $23 + 30i$ where i is the PRT block index ranging from 0 to $M - 1$. The number of transmitted blocks, M, corresponds to the dwell time for measurements and also is the length of the time series. There are 30 sample times and thus 30 possible time series that correspond to the normalized integer times that occur during one block of PRTs. However, sampling of the returning echoes can not happen simultaneously with pulse transmission and therefore only $30 - 4 = 26$ total times series are gathered for this SMPRF code. Note that a sample time of 150μs after a transmit pulse corresponds to a range of $cT/2 = 22.5$km and therefore the normalized sample times of 20 and 21 occur at ranges 450 km and 472.5 km respectively. When a transmit pulse is more than 20 normalized time units from a sample time, there are no resulting return echoes, i.e., 460 km is considered to be the maximum possible range for weather echo return. The arrows in Fig. 1 show that return echo is received at time $t = 1$ due to the indicated transmit pulses. The transmit pulses at times $t = -25$ and -30 do not contribute since they occurred more than 20 time units before the $t = 1$ sample time. The time series sample at $t = 1$ is written

$$V_1(1) = \beta_1^{(5)}(1) + \beta_8^{(7)}(1) + \beta_{18}^{(10)}(1) \tag{2}$$

where the subscript indicates the sample time in normalized time units which corresponds to the range resolution volume and the superscript indicates the pulse PRT in normalized time units which illuminates the resolution volume. The "(1)" indicates that it is the first sample of the time series. For example, $\beta_8^{(7)}(1)$ represents the first time series element in the return time series corresponding to the 8^{th} resolution volume which is illuminated by a pulse with PRT length of 7 (normalize time units). The 8^{th} resolution is located at $CT/2 = C\,8(150\mu\text{s})/2 = 180$ km range. As the block of PRTs is repeated, additional time series samples are gathered. For the time series in Eq. (2) additional time series samples are gathered at $t = 1 + 30i$, $i = 1$ to $M - 1$. The time series corresponding to the sample times $t = 1+30i$, $i = 0$ to $M-1$ is written as,

$$\begin{aligned} V_1(1 + 30i) &= \beta_1^{(5)}(1 + 30i) + \beta_8^{(7)}(1 + 30i) \\ &\quad + \beta_{18}^{(10)}(1 + 30i) \end{aligned} \tag{3}$$

and with the index understood as

$$V_1 = \beta_1^{(5)} + \beta_8^{(7)} + \beta_{18}^{(10)} \tag{4}$$

Similarly, the time series corresponding to sample time $t = 2$ consists of samples collected at $t = 2 + 30i$, $i = 0$ to $M - 1$ and is written as,

$$V_1 = \beta_2^{(5)} + \beta_9^{(7)} + \beta_{19}^{(10)} \tag{5}$$

Continuing in this way, a set of time series equations is constructed:

$$\begin{aligned}
V_1 &= \beta_1^{(5)} + \beta_8^{(7)} + \beta_{18}^{(10)} \\
V_2 &= \beta_2^{(5)} + \beta_9^{(7)} + \beta_{19}^{(10)} \\
V_3 &= \beta_3^{(5)} + \beta_{10}^{(7)} + \beta_{20}^{(10)} \\
V_4 &= \beta_4^{(5)} + \beta_{11}^{(7)} \\
V_5 &= \text{No data} \\
V_6 &= \beta_1^{(8)} + \beta_6^{(5)} + \beta_{13}^{(7)} \\
V_7 &= \beta_2^{(8)} + \beta_7^{(5)} + \beta_{14}^{(7)} \\
V_8 &= \beta_3^{(8)} + \beta_8^{(5)} + \beta_{15}^{(7)} \\
V_9 &= \beta_4^{(8)} + \beta_9^{(5)} + \beta_{16}^{(7)} \\
V_{10} &= \beta_5^{(8)} + \beta_{10}^{(5)} + \beta_{17}^{(7)} \\
V_{11} &= \beta_6^{(8)} + \beta_{11}^{(5)} + \beta_{18}^{(7)} \\
V_{12} &= \beta_7^{(8)} + \beta_{12}^{(5)} + \beta_{19}^{(7)} \\
V_{13} &= \text{No data} \\
V_{14} &= \beta_1^{(10)} + \beta_9^{(8)} + \beta_{14}^{(5)} \\
V_{15} &= \beta_2^{(10)} + \beta_{10}^{(8)} + \beta_{15}^{(5)} \\
V_{16} &= \beta_3^{(10)} + \beta_{11}^{(8)} + \beta_{16}^{(5)} \\
V_{17} &= \beta_4^{(10)} + \beta_{12}^{(8)} + \beta_{17}^{(5)} \\
V_{18} &= \beta_5^{(10)} + \beta_{13}^{(8)} + \beta_{18}^{(5)} \\
V_{19} &= \beta_6^{(10)} + \beta_{14}^{(8)} + \beta_{19}^{(5)} \\
V_{20} &= \beta_7^{(10)} + \beta_{15}^{(8)} + \beta_{20}^{(5)} \\
V_{21} &= \beta_8^{(10)} + \beta_{16}^{(8)} \\
V_{22} &= \beta_9^{(10)} + \beta_{17}^{(8)} \\
V_{23} &= \text{No data} \\
V_{24} &= \beta_1^{(7)} + \beta_{11}^{(10)} + \beta_{19}^{(8)} \\
V_{25} &= \beta_2^{(7)} + \beta_{12}^{(10)} + \beta_{20}^{(8)} \\
V_{26} &= \beta_3^{(7)} + \beta_{13}^{(10)} \\
V_{27} &= \beta_4^{(7)} + \beta_{14}^{(10)} \\
V_{28} &= \beta_5^{(7)} + \beta_{15}^{(10)} \\
V_{29} &= \beta_6^{(7)} + \beta_{16}^{(10)} \\
V_{30} &= \text{No data}
\end{aligned} \tag{6}$$

It is possible to solve this set of simultaneous time series equations for the mean power of each of the resolution volumes, $|\beta_j^{(i)}|^2$.

As shown in (Pirtilla et al. 2005) and following the steps in the derivation of the maximum unambiguous velocity for the staggered PRT algorithm described above (Zrnić and Mahapatra 1985), the maximum unambiguous velocity for the SMPRF algorithm is given by,

$$v_{a,SMPRF} = \pm \frac{\lambda}{4min\left\{PRT_i - PRT_j\right\}}; i \neq j \quad (7)$$

For the SMPRF$_{(150);5,8,10,7}$ code with $\Delta_t = 150\mu s$, this yields $v_{a,SMPRF} = 89.33ms^{-1}$. This value corresponds to a velocity of about 200 miles per hour which is more than adequate for the measurement of weather phenomena.

2.1 *Mean Power Estimation*

In the following sections, we adopt the following notation: P represents the true power value, $\tilde{P}$ represents the estimated mean power value prior to the inversion process, and $\hat{P}$ represents the mean power estimate after the inversion process.

The mean estimated power for the i^{th} volume corresponding to the j^{th} PRT is,

$$\begin{aligned} \tilde{P}_i &= \frac{1}{M}\sum_{k=1}^{M}\left|\beta_i^{(j)}(k)\right|^2; j \in \{5,7,10,8\}, \\ & \quad i \in \{1,2,...,20\} \end{aligned} \quad (8)$$

The total estimated power $\tilde{Z}_1$ corresponding to the time series V_1 is written as,

$$\begin{aligned} \tilde{Z}_1 &= \frac{1}{M}\sum_{k=1}^{M}|V_1|^2 \\ &= \frac{1}{M}\sum_{k=1}^{M}\left|\beta_1^{(5)}(k) + \beta_8^{(7)}(k) + \beta_{18}^{(10)}(k)\right|^2 \end{aligned} \quad (9)$$

As a consequence of the independence between measurement volumes all cross products are assumed 0 (Bringi and Chandrasekar 2001) and Eq. (9) reduces to,

$$\begin{aligned} \tilde{Z}_1 &= \frac{1}{M}\sum_{k=1}^{M}\left|\beta_1^{(5)}(k)\right|^2 \\ &+\frac{1}{M}\sum_{k=1}^{M}\left|\beta_8^{(7)}(k)\right|^2 + \frac{1}{M}\sum_{k=1}^{M}\left|\beta_{18}^{(10)}(k)\right|^2 \\ &= \tilde{P_1} + \tilde{P_8} + \tilde{P_{18}} \end{aligned} \quad (10)$$

Thus, the equations for the total estimated powers, $\tilde{Z_n}; n \in \{1,2,...,30\}$ corresponding to Eqs. (6) can be written in matrix notation as,

$$\tilde{\mathbf{Z}} = \mathbf{A}\tilde{\mathbf{P}} \quad (11)$$

where $\tilde{\mathbf{Z}}$ is the vector of estimated power measurements, $\mathbf{A}$ is the code matrix describing the signal overlays, with $\mathbf{A_{i,j}} \in \{0,1\}$, and $\tilde{\mathbf{P}}$ is the vector of calculated mean powers from each measurement range.

Since the row space of the inversion matrix, $\mathbf{A}$, is greater than its column space, the system of equations is over-determined. The Moore-Penrose pseudo-inverse is used to solve this set of equations, yielding the recovered mean power vector, $\hat{\mathbf{P}}$.

As seen in Eqs. (6), there are either three or four time series constructed for each resolution volume depending on the number of PRTs that illuminate the resolution volume. For example, for the resolution volume corresponding to normalized sample time 1, the four time series are $\beta_1^{(5)}$, $\beta_1^{(7)}$, $\beta_1^{(10)}$, and $\beta_1^{(8)}$, i.e., one time series corresponding to each PRT in the block of PRTs used. Since these time series are samples from the same assumed statistically stationary medium, the mean power estimates become equal in the limit of M (Bringi and Chandrasekar 2001), i.e.,

$$\begin{aligned} \frac{1}{M}\sum_{k=1}^{M}\left|\beta_1^{(5)}(k)\right|^2 &= \frac{1}{M}\sum_{k=1}^{M}\left|\beta_1^{(7)}(k)\right|^2 \\ &= \frac{1}{M}\sum_{k=1}^{M}\left|\beta_1^{(10)}(k)\right|^2 \\ &= \frac{1}{M}\sum_{k=1}^{M}\left|\beta_1^{(8)}(k)\right|^2 \end{aligned} \quad (12)$$

However, when calculating the average powers for finite-length time series, these estimates will not be equal since they are estimated from different samples separated in time.

To illustrate this point, consider the first and sixth equations in the set of measurement equations for the SMPRF$_{(150);5,8,10,7}$ code, with time series time indices, k, removed for convenience,

$$\begin{aligned} V_1 &= \beta_1^{(5)} + \beta_8^{(7)} + \beta_{18}^{(10)} \\ V_6 &= \beta_1^{(8)} + \beta_6^{(5)} + \beta_{13}^{(7)} \end{aligned} \quad (13)$$

where $\beta_1^{(5)}$ and $\beta_1^{(8)}$ are two time series for resolution volume 1. The mean powers corresponding to $\beta_1^{(5)}$ and $\beta_1^{(8)}$ are assumed equal in the matrix inversion process for recovery of the mean power estimates. The difference

in estimated average power values from these two time series will cause errors in the power recovery process. As will be shown, these errors can be quite large and bias the mean power estimates, $\hat{P}$.

2.2 *Mean Velocity Estimation*

The SMPRF velocity recovery is based on the estimation of unequally time spaced lags of the autocorrelation function of the time series for each resolution volume. Consider $\beta_1^{(5)}$, $\beta_1^{(7)}$, and $\beta_1^{(10)}$, $\beta_1^{(8)}$, which which are the time series for the first resolution volume. Fig. 2 shows the individual time series that results from two blocks of SMPRF$_{(150);5,8,10,7}$ code. The arguments of the time series are given in normalized time units. These four time series can be used to calculate various lags of the auto correlation function of β_1. For example consider the time series $\beta_1^{(5)}$ and $\beta_1^{(7)}$. Part of the auto correlation function of β_1 can be calculated as,

$$R_1(5+k30) \quad = \quad \sum_{i=0}^{M-1} \beta_1^{(5)}(i30)\beta_1^{(7)}(5+(i+k)30) \tag{14}$$

Thus, the autocorrelation lags that can be calculated from this product are $5+k30$ where k can range from $-(M-1)$ to $M-1$.

Again, time series from different resolution volumes are independent and their cross correlation is zero in the limit of M. However, for finite length time series, these cross correlation products will not be zero and generate "noise". This noise is a limiting factor for the mean velocity recovery process. As will be illustrated later in this report, the variance of the noise term in the equations above depends upon the amount of overlaid power.

The range of lag values estimated and used in the estimation of the mean velocity using the SMPRF algorithm is limited by the coherence time. Coherency time, T_D, is defined as the time for which magnitude of the autocorrelation drops to e^{-1} (Bringi and Chandrasekar 2001) and is given by,

$$T_D = \frac{\lambda}{2\sqrt{2}\pi\sigma_v} \tag{15}$$

The block length of the SMPRF$_{(150);5,8,10,7}$ code is 4.50 ms. For a radar operating at C-band (for this study, $\lambda = 5.6cm$) and a weather signal spectrum width of 2 ms, the coherence time is 3.01 ms. For a spectrum width of 4 ms^{-1}, the coherence time drops to 1.51 ms. Given these parameters, we choose to constrain the limits of ACF lags

Volume(i)	Lag Values(n)
1,2,3,4,9	5, 7, 8, 10, 13
5,13	8, 10, 12
6	5, 7, 8, 10
7,12	5, 8, 13
8,18	7, 10, 13
10,17	5, 7, 12
11	5, 7, 8, 10, 12
14,15,16,19	5, 7, 8, 10, 12, 13
20	5, 8

Table 1: *ACF lag values computed using SMPRF$_{(150);5,8,10,7}$ code.*

used in the estimation of the mean velocity to 15 in normalized time, or 15 X 150μs = 2.25 ms. Empirical SMPRF simulations show that good velocity recovery performance was attained when used ACF lags are within about 75% of the coherence time. Thus for the following simulation studies of SMPRF$_{(150);5,8,10,7}$, ACF lag times less than 2.25 ms are used for velocity recovery.

Using the example SMPRF$_{(150);5,8,10,7}$ code, the set of ACF lag values available for each resolution volume is given in Table 1. As seen in Table 1, different resolution volumes will have both different number of available AFC lags as well as different ACF lags. Note that the lack of radar capability to receive while transmitting accounts for the lower number of recovered ACF lags in certain volumes.

Once the ACF lag values are estimated, the mean velocity is then estimated. Next, a technique for velocity estimation is examined in the following section.

2.3 *Spectral Maximum Technique*

The technique used in (Pirtilla et al. 2005) to estimate mean velocity from unevenly sampled ACF lag values uses the Discrete Fourier Transform (DFT) of the interpolated ACF. Missing values of the AFC are interpolated with zeros and the DFT is then taken. The location of the peak of the power spectrum is taken to be the estimate for the mean velocity (Roberts and Mullis 1987).

The power spectrum is calculated as,

$$\tilde{S}_i[k] = \sum_{n=0}^{N-1} \tilde{R}_i(n)\, e^{-\frac{2\pi j}{N}nk}; k = 0, ..., N-1 \tag{16}$$

where N is the number of points used in the DFT calculation.

The following simulation illustrates this velocity estimation technique. In Fig. 3, the power spectrum (zero

padding is used so that $N_{FFT} = 512$) of a simulated 64-point weather signal is shown, with $\sigma_v = 2\ m/s$, $v = 30\,m/s$, $SNR = \infty$, and $PRT = 150\,\mu s$. Then, the ACF of the simulated signal is calculated. The unevenly spaced samples of the ACF of the signal calculated are obtained by selecting the desired ACF values according to Table 1. All other ACF lags are set to zero. This is equivalent to multiplying the calculated ACF function by a binary mask, $M_1[k]$, which is given by,

$$M_1[k] = \{1\,0\,0\,0\,0\,1\,0\,1\,1\,0\,1\,0\,0\,1\} \tag{17}$$

where $M_1[-k] = M_1[k]$. The member of the autocorrelation function can be listed as

$$\begin{aligned} R_1[k] \;=\; & \{\hat{P}_1\ 0\ 0\ 0\ 0\ R_1[5]\ 0\ R_1[7]\ R_1[8] \\ & 0\ R_1[10]\ 0\ 0\ R_1[13]\} \end{aligned} \tag{18}$$

where $\hat{P}_1$ is the mean power estimate and $R_1[-k] = R_1^*[-k]$. The power spectrum of the binary masking sequence is shown in Fig. 4. Mathematically, the power spectrum of the unevenly spaced ACF spectrum, $\mathbf{S_1}$ is formed by the convolution of the weather power spectrum, $\mathbf{X}$, and binary mask spectrum, $\mathbf{M}$ as,

$$\tilde{\mathbf{S}}_\mathbf{1} = \mathbf{M_1} \odot \mathbf{X} \tag{19}$$

where $\odot$ denotes convolution.

The power spectrum of the simulated weather signal, which is the DFT of $R_1[k]$, is shown in Fig. 5. Comparing Fig. 5 to Fig. 3, it is seen that the peak of the spectra of Fig. 5 gives the velocity of about $\hat{v} = 28.6\,\mathrm{ms}^{-1}$.

3. SIMULATION OVERVIEW

The time series simulation technique is described in Chandrasekar et al. (1986). For each range volume, a time series, α, is generated with time spacing equal to the greatest common divisor of PRTs, in this case, $\Delta_t = 150\ \mu s$. The time series simulation length is equal to the length of the SMPRF code times the number of PRT blocks transmitted. In the case of the SMPRF$_{(150);5,8,10,7}$ code with 15 blocks transmitted, the dwell time is $30 \times 15 = 450 \times 150\ \mu s = 67.5ms$. The time series, $\beta_i^{(j)}$,corresponding to the i^{th} volume corresponding to the j^{th} PRT are selected subsets of the time series α, with one element selected from each block and are thus spaced one code length apart (in this case, 4.5 ms). For example, for $\beta_6^{(7)}$, the time series corresponding to the6^{th} measurement volume relative to the pulse of length 7 normalized time units, i.e., the 4^{th} PRT in the SMPRF$_{(150);5,8,10,7}$ code, is $\beta_6^{(7)} = \{\alpha_{29}, \alpha_{59}, \alpha_{89}, ..., \alpha_{449}\}$. Again, the length of these return time series are equal to the number of code blocks transmitted. This simulation procedure ensures proper time spacing and correlation between the time series constructed for a volume.

In order to evaluate the mean power and velocity recovery statistics, an input power versus range profile is selected. The recovery statistics will vary according to the input power range profile chosen and we give three example profiles here that demonstrate the expected quality of the recovered power and velocity. The three power profiles are: a flat profile with all ranges set to 20 dBZ, a single-peak triangular profile with 50 dBZ power level separation, and a double-peak triangular profile with 15 dBZ power level separation. The SNR in each case is infinite. It was shown through simulation that the performance of the mean velocity estimation is independent of the input mean velocity value, between $-v_a$ and $+v_a$ and thus, a flat mean velocity profile was selected for input with velocity value set to $v_a/2$. A spectrum width of 2 m s^{-1} is selected for all ranges. The radar frequency is 5.6 GHz ($\lambda = 5.36\ cm$). Fifteen blocks are used for the SMPRF$_{(150);5,8,10,7}$ code, which translates to a dwell time of 67.5 ms and two hundred iterations were run to generate statistics. In the figures illustrating mean power and mean velocity profile recovery, the vertical box dimension represents one standard deviation while the horizontal line within the box marks the mean estimate. The input power and velocity profiles are displayed in each case, superimposed to illustrate the corresponding power separation between ranges.

3.1 *Simulation Results*

The simulation results for the estimation of mean power and velocity values using the SMPRF$_{(150);5,8,10,7}$ code with maximum unambiguous measurement range of 460 km are seen in Fig. 6 through Fig. 11. For the 20 dBZ flat input power profile, Fig. 6 shows unbiased mean power recovery with standard deviation values around 4 dBZ for each measurement range. Fig. 7 shows biased mean velocity recovery performance with standard deviations between 30 and 40 ms^{-1}. Reasons for this behavior are described in the next section.

For the 50 dBZ triangular input power profile, Fig. 8 shows unbiased mean power recovery and standard deviation values less than 5 dB in those ranges with powers 35 dBZ and above. For those ranges with less power, the performance is biased with standard deviation values between 10 and 15 dB. Fig. 9 shows unbiased mean velocity recovery and standard deviation values less than 0.1 ms^{-1} for the ranges whose powers are 35 dBZ and above. Measurements in ranges whose power values are below 35 dBZ exhibit biasing and standard deviation values between 40 and 50 ms^{-1}. These results suggest the ranges with lesser power are being dominated by the noise generated in the correlation process.

For the 15 dBZ double triangular input power profile, Fig. 10 shows unbiased performance and standard deviations which increase from less than 1 dB to around 8 dB as the power separation between measurement ranges increases. Fig. 11 shows biasing of the mean velocity estimates as the power separation between measurement ranges increases and standard deviation values increasing from about 10 ms^{-1} to about 50 ms^{-1}.

The results show that the $\mathrm{SMPRF}_{(150);5,8,10,7}$ code scheme can recover reasonable power estimates only for those resolution bins with the highest power. When the power of a resolution bin drops to about 15 to 20 dB below the highest power bin, the standard deviation of the power measurements can become 3dB and much greater depending on the simulated power range profile. The recovered velocities only look reasonable for the triangular power profile of Fig. 9 for the higher power resolution volumes. In all other locations, the recovered velocities have large biases and standard deviations. Reasons for these effects are illustrated and discussed in the following section.

a. *Effect of finite-length time series*

The received voltage at the radar is a complex stochastic signal, considered as one realization of the underlying stochastic process. Physically, the stochastic process is driven by the reshuffling of the precipitation particles during the dwell time of the radar (Bringi and Chandrasekar 2001). The stochastic process is considered stationary so that the mean of the time series of the magnitude squared voltage is proportional to power. Since the complex voltages (time series) are finite in length, the mean of the magnitude squared voltage is an estimate of the true power. It is well known that this power estimate has unbiased mean and standard deviation which depends upon the spectrum width. In the SMPRF algorithm, multiple time series representations for a resolution volume are created. For example, for resolution volume 1 for $\mathrm{SMPRF}_{(150);5,8,10,7}$, the time series are $\beta_1^{(5)}$, $\beta_1^{(8)}$, $\beta_1^{(10)}$, $\beta_1^{(7)}$. Even though these time series are from the same resolution volume and are correlated (depending on the spectrum width), the mean power estimates are not equal, in general. Since the matrix inversion process is based on the equality of these powers (i.e., Eq. (12) holds true for each resolution volume), this power inequality produces errors in the mean power estimates. Power values for each of the 20 resolution volumes using the $\mathrm{SMPRF}_{(150);5,8,10,7}$ code can appear up to a maximum of 4 times in the inversion equation, as shown by Eq. (6). Thus, this assumption of power equality of time series from the same resolution volume is one source of error in the power recovery process. Another error source in SMPRF power recovery due to finite-length time series is the assumption that the cross products of the power calculation in Eq. (12) are zero. In the following analysis, these two error sources are separated and quantified.

Eqs. (9) and (10) are written under the assumption that the cross-power terms between the resolution volumes are equal to zero, i.e,

$$\left| \sum_k \beta_i^{(j)}(k) \beta_n^{(l)}(k) \right|^2 = 0; i \neq n \tag{20}$$

For finite-length time series, this will not be true. To illustrate this error source, the simulation procedure is changed. Return time series are still generated, but this time, the mean power values of each time series are calculated individually before being overlaid and separated by the inversion process. instead, power values were generated, overlaid, and separated by the inversion process. This eliminates contributions to the total power due to the cross products of the time series. The results for this simulation using the 50 dBZ triangular profile described above are shown in Fig. 12. Fig. 12 illustrates error in the recovery of the mean powers using the SMPRF algorithm when the time series cross-correlation terms between resolution volumes are set to 0. The results shown in Fig. 12 are similar to those in Fig. 8. This suggests the cross-correlation terms are a secondary source of error in the SMPRF mean power recovery process at least for the simulations parameters used here.

To quantify the expected power difference between the four power estimates for a particular resolution volume, 50,000 time series simulations were run for a spectrum width of 4 ms^{-1}. For each simulation, the six pairwise power ratios are calculated:

$$\begin{aligned} P(i,j) &= 10 \log_{10} \Big[\frac{|\beta_1^i|^2}{|\beta_1^j|^2} \Big]; \\ & \quad i, j \in 1,\, 2,\, 3,\, 4,\, i \neq j \end{aligned} \tag{21}$$

where the "i" and "j" stand for the PRTs 750 μs, 1200 μs, 1500 μs, and 1250 μs. The mean and standard deviation are calculated for each ratio. The mean ratios are 1 (0 dB) as expected. The standard deviations are given in Table 2. For the used simulation parameters, the average standard deviation is about 1 dB or 25%.

Next, the power of the time series that represent the same resolution volume are forced to be equal so that the sole error source is now power from the cross product terms. The time series are scaled such that equality exists between the mean power estimates made from each of the time series according to the following equation,

$$\tilde{\beta}_i^{(j)} = \sqrt{\frac{P_i}{\hat{P}_i}} \beta_i^{(j)} \tag{22}$$

PRT	750 μs	1200 μs	1500 μs	1250 μs
750 μs	0	0.8682	1.1705	0.6889
1200 μs	0.8682	0	1.0186	0.9854
1500 μs	1.1705	1.0186	0	0.9578
1250 μs	0.6889	0.9854	0.9578	0

Table 2: *Standard deviation of mean power estimates, in dB, used in the matrix inversion process for first resolution volume for the 50 dBZ triangular power profile.*

where P_i is the input (true) power at measurement range i and $\hat{P}_i$ is the calculated power at measurement range i. This scaling eliminates the differences in inversion variables and isolates the finite-length time series effects. The results of this simulation using the 50 dB triangular power profile are shown in Fig. 13. As can be seen, the recovery performance of the mean powers has improved as compared to Fig. 12 This again indicates that inequality of the powers of the time series is the dominant source of error in the SMPRF algorithm for the simulation parameters used.

4. CONCLUSIONS

The simultaneous multiple pulse repetition frequency (SMPRF) for range-velocity ambiguity mitigation was evaluated via time series simulations. Time series corresponding to several modeled power range profiles were simulated for each range resolution volume, overlaid according to the radar pulsing scheme and then the SMPRF algorithm was applied to recovery the known simulated mean powers and velocities. The recovered powers and velocities were compared to the true simulated powers and velocities so that biases and standard deviations could be calculated. The wave length used for the simulations was 5.6 cm but the results are general enough so that the performance of the SMPRF algorithm at other wave lengths can be judged.

The simulations studies show that there are indeed limitation to the SMPRF technique and these limitations can be severe. In general it was shown that separation and recovery of overlaid echoes is only good for power ratios less than about 15 dB depending on the SMPRF code used and the number of overlaid echoes. When there is significant echo overlay along the radar radial, good velocity estimates are only available for the highest power resolution volumes and even this untrue for some of the simulated radar reflectivity profiles presented.

The theory behind the SMPRF algorithm does show that unlimited unambiguous range and velocity can be obtained when the analysis is done with expectations of random variables that model the stochastic process of weather radar signals. Ensemble statistical properties, such as the correlation product of two independent, uncorrelated processes is zero, are used in the theoretical development; however, for finite length time series representations of these processes, such correlation products are in general not zero and must be taken in to account. For example, consider the SMPRF matrix inversion process for recovering radar power. For the SMPRF$_{(150);5,8,10,7}$ coded analyzed, there are typically four times series representations of the statistical processes of a common resolution volume corresponding to each of the four PRTs used. Even though these time series are measured in close time proximity and are correlated, their mean powers are in general not equal. The degree of power inequality depends upon the spectrum width of the weather echo and the radar times series length. For typical radar measurement parameters of dwell time of 64 ms and a spectrum width of 4 ms^{-1}, the mean power differences among the four time series is about 1dB or 25%. The SMPRF matrix inversion process assumes that these powers are equal. This is likely the limiting factor in the power recovery process for most realistic weather range profiles. However, If spectrum widths are very narrow, the assumption that the cross terms in the correlation products are zero may become the dominate source of error rather than the assumption of equality of powers of time series that represent the same resolution volume.

The SMPRF velocity recovery technique is limited by a similar mechanism. Several "first lag" estimates of the auto correlation function for a radar resolution volume are possible since each resolution volume has four time series representations for the case of SMPRF$_{(150);5,8,10,7}$. Correlating these time series yields several unequally spaced estimates of the auto correlation function. As shown, each time series gathered at particular sample time can also contain echoes from several resolution volumes. Since the overlaid echoes are from physically separate resolution volumes, the overlaid time series are independent and their cross correlations are zero, at least asymptotically. Since the time series are finite, these cross correlations are not zero and in effect mask the desired "first lag" correlation in noise proportional to the strength of the overlaid echoes. This "correlation noise" then limits the accuracy of the recovered velocities. The extent of the limitation depends on the number of overlaid echoes and their strength. For the SMPRF$_{(150);5,8,10,7}$ algorithm analyzed, if there are significant overlaid echoes throughout the radar range (for example see Figure 6), the velocities are recovered well nowhere.

Acknowledgment
This work was supported by Vaisala, Inc. E. Ruzanski and V. Chandrasekar were also supported via the Engineering Research Centers Program of the National Sci-

ence Foundation under NSF award number 0313747. We would also like to thank Greg Meymaris for the insightful technical discussions. The National Center for Atmospheric Research is sponsored by the National Science Foundation. Any opinions, findings and conclusions or recommendations expressed in this publication are those of the author(s) and do not necessarily reflect the views of the National Science Foundation.

References

Bringi, V. and V. Chandrasekar, 2001: *Polarimetric Doppler Weather Radar*. Cambridge Univ. Press, Cambridge, UK.

Pirtilla, J., M. Lehtinen, A. Huuskonen, and M. Markkanen, 2005: A proposed solution to the range-Doppler dilemma of weather radar measurements by using the SMPRF codes, practical results, and a comparison with operational measurements. *J. Appl. Meteor.*, **44**, 1375–1390.

Roberts, R. and C. Mullis, 1987: *Digital Signal Processing*. Addison-Wesley, New York, 578 pp.

Zrnić D.S., P.R. Mahapatra, 1985: Two methods of ambiguity resolution in pulse Doppler weather radars. *IEEE Trans. Aerosp. Electron. Syst.*, **AES-21**, 470–483.

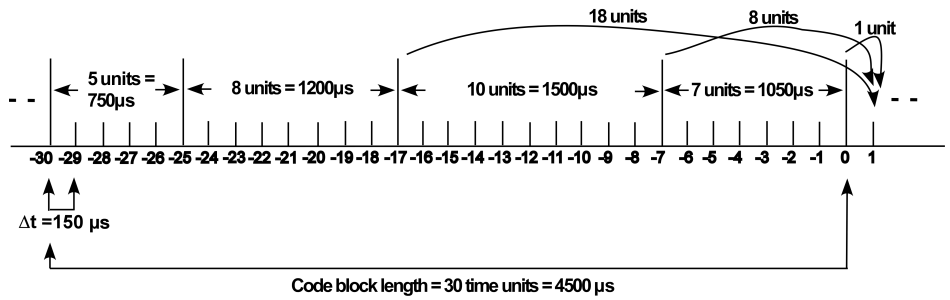

Figure 1: *Illustration and operation of the SMPRF code; 5, 8, 10, 7 PRTs,* $\Delta_t = 150\mu s$.

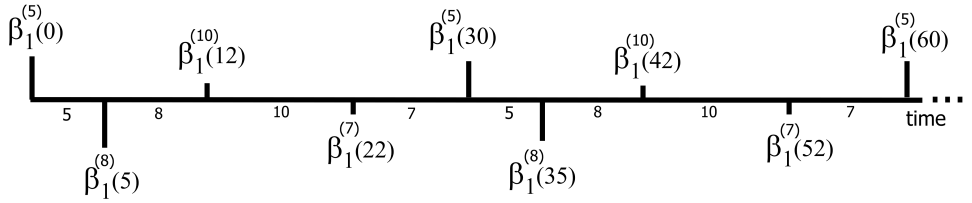

Figure 2: *Diagram of the four time series for resolution volume one for* $SMPRF_{(150);5,8,10,7}$ *code. The argument of the time series members is in normalized time units.*

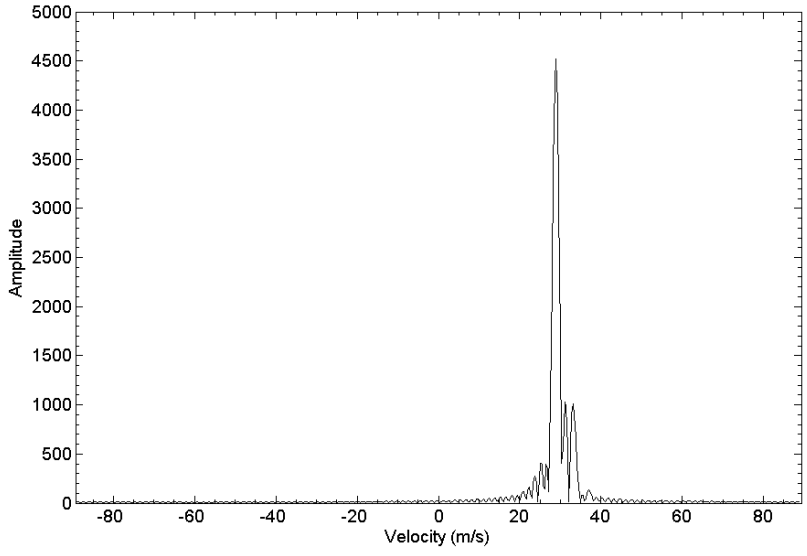

Figure 3: *Velocity spectrum of simulated weather signal.*

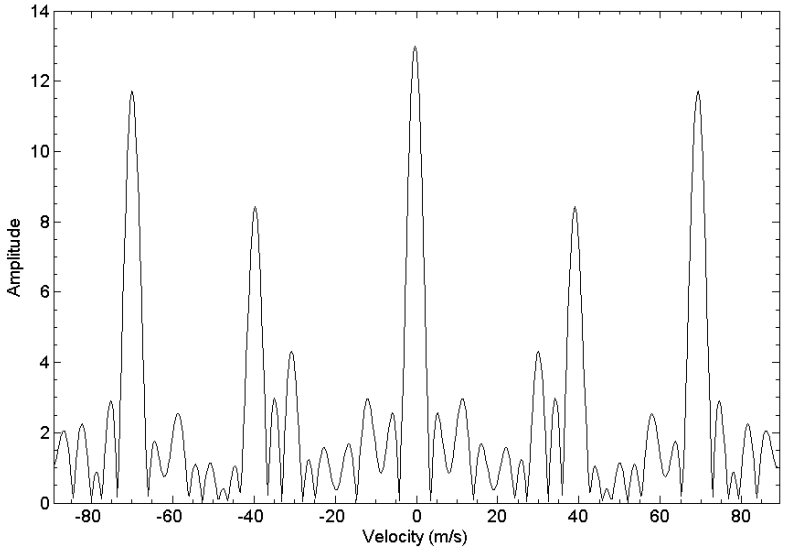

Figure 4: *Power spectrum of binary mask sequence.*

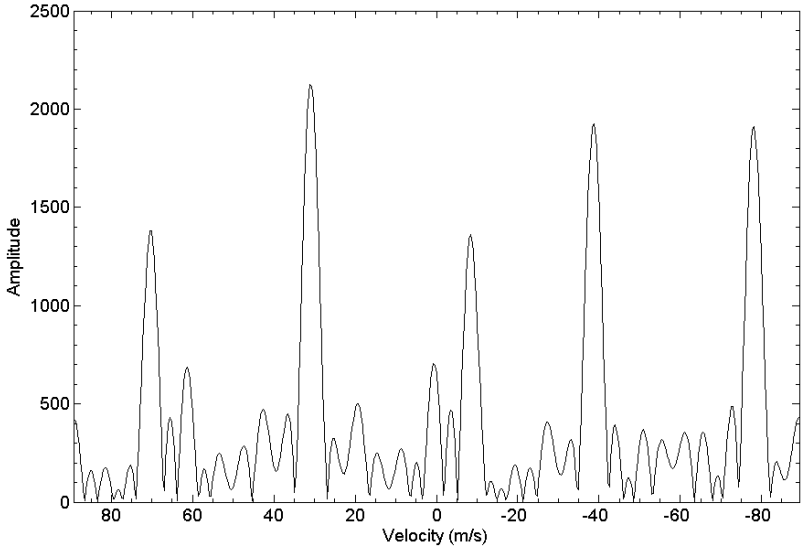

Figure 5: *Power spectrum of weather signal recovered using the SMPRF*$_{(150);5,8,10,7}$ *code,* $SNR = \infty$.

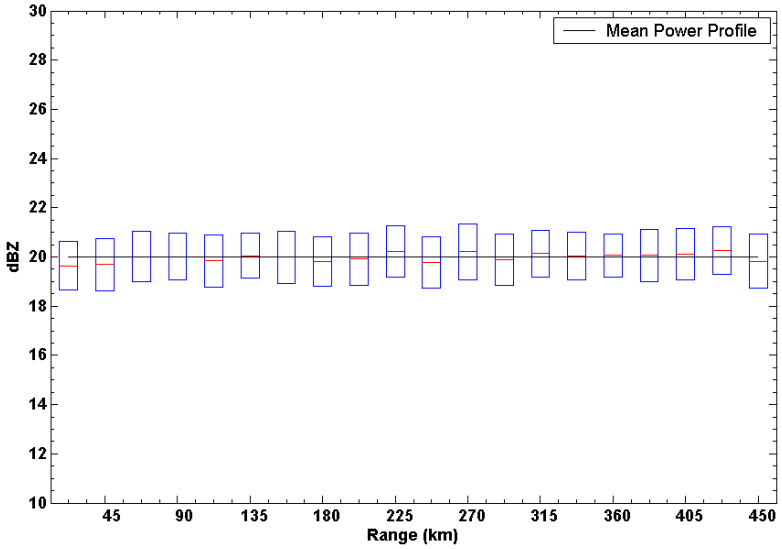

Figure 6: *Mean power profile recovery for 20 dBZ flat profile, SMPRF*$_{(150);5,8,10,7}$ *code.*

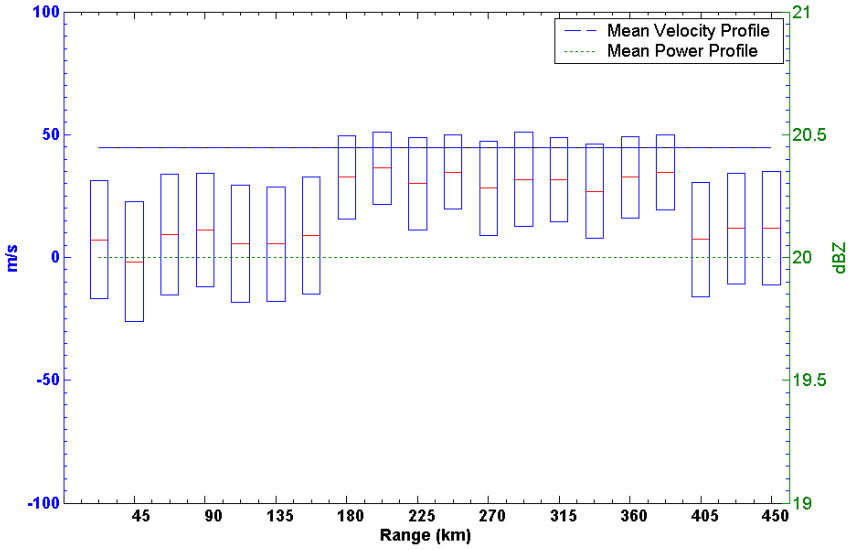

Figure 7: *Mean velocity profile recovery for 20 dBZ flat profile, SMPRF*$_{(150);5,8,10,7}$ *code.*

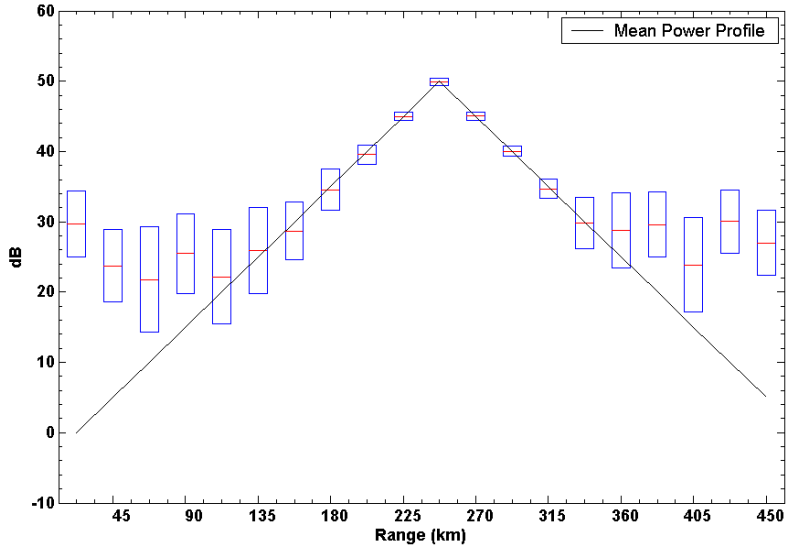

Figure 8: *Mean power profile recovery for 50 dBZ triangular profile, SMPRF$_{(150);5,8,10,7}$ code.*

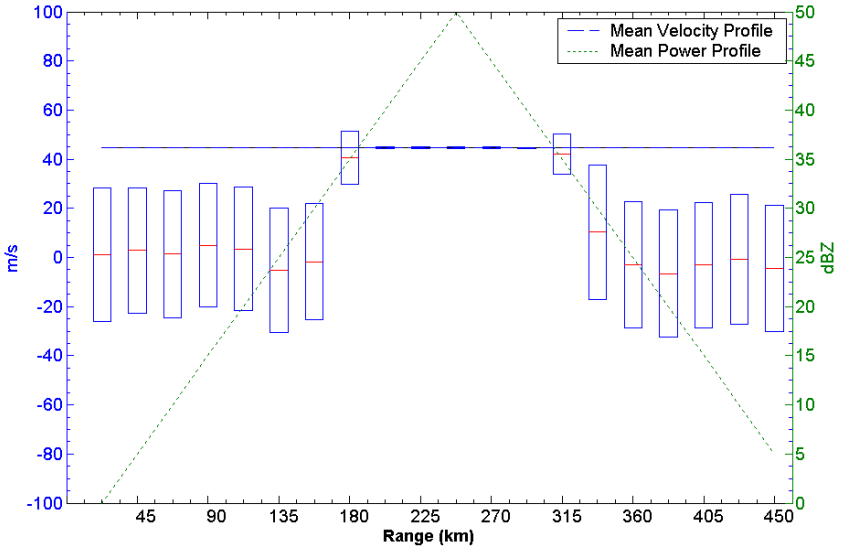

Figure 9: *Mean velocity profile recovery for 50 dBZ triangular profile, SMPRF$_{(150);5,8,10,7}$ code.*

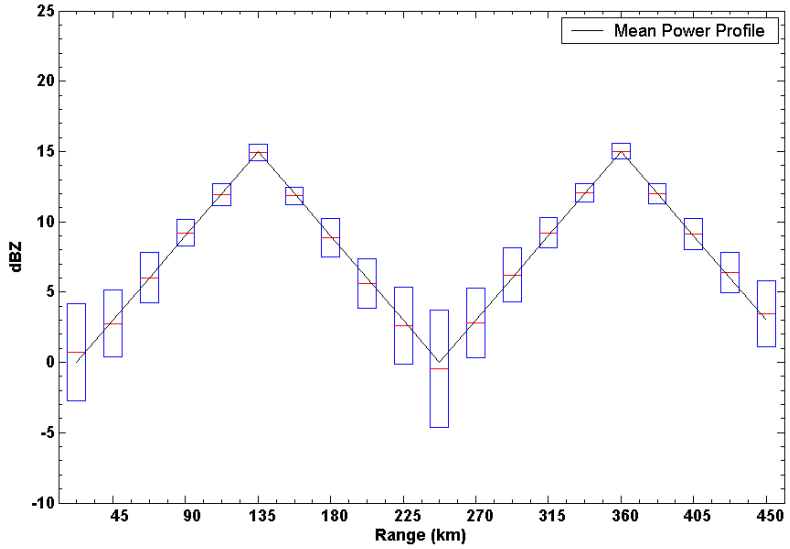

Figure 10: *Mean power profile recovery for 15 dBZ triangular profile, SMPRF*$_{(150);5,8,10,7}$ *code.*

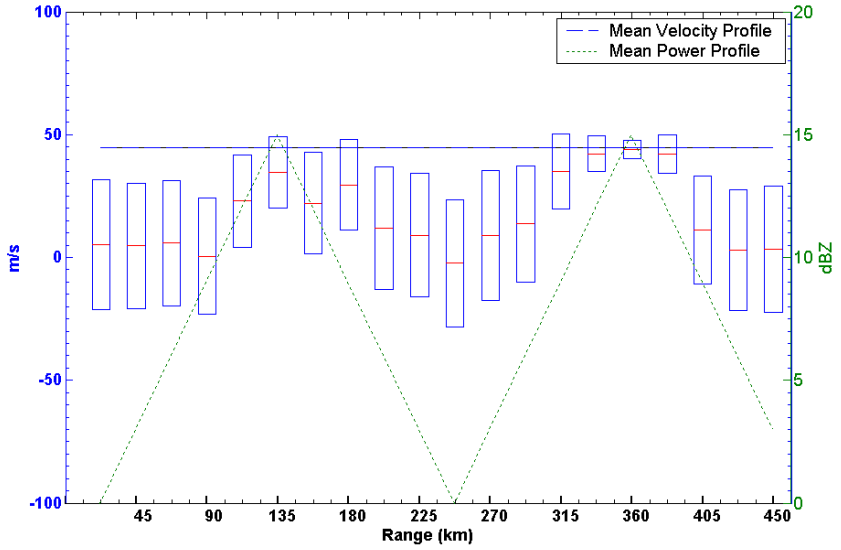

Figure 11: *Mean velocity profile recovery for 15 dBZ triangular profile, SMPRF*$_{(150);5,8,10,7}$ *code.*

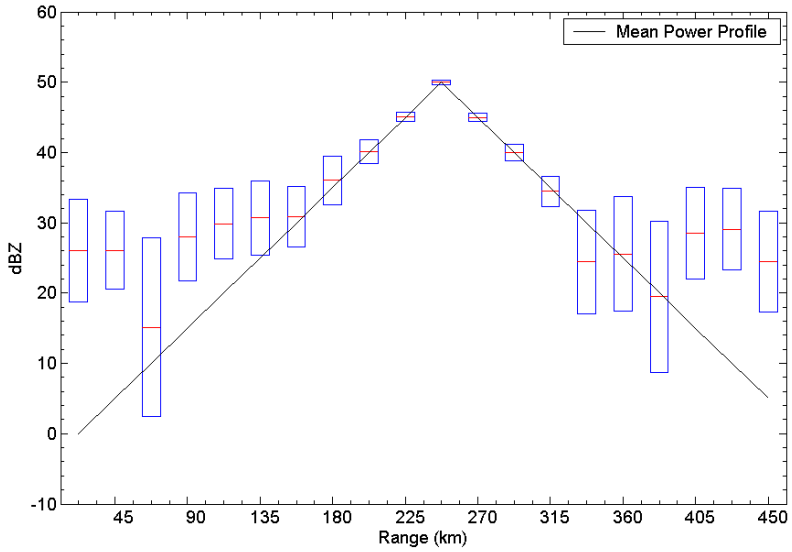

Figure 12: *Mean power profile recovery for 50 dBZ triangular profile, SMPRF$_{(150);5,8,10,7}$ code, using point power values.*

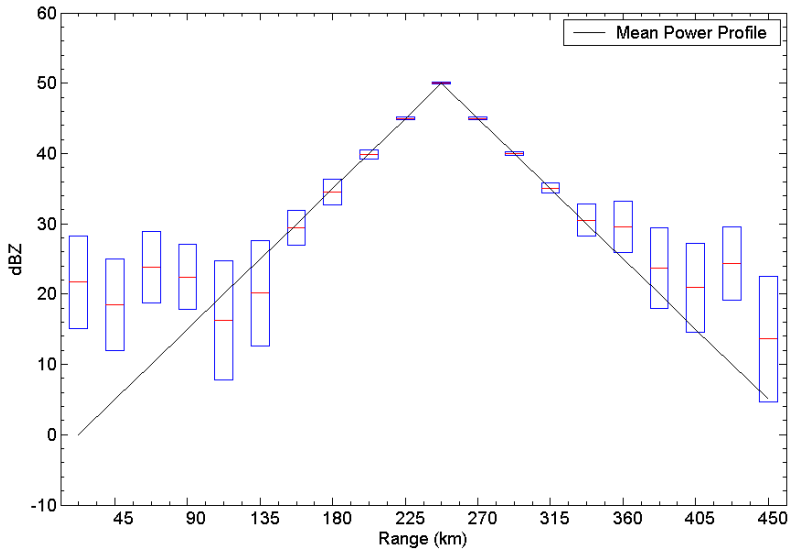

Figure 13: *Mean power profile recovery for 50 dBZ triangular profile, SMPRF$_{(150);5,8,10,7}$ code, using scaled time series.*